Explaining glomerular pores with fiber matrices

A visualization study based on computer modeling

James W. Booth and Charles J. Lumsden
Membrane Biology Group and Department of Medicine, University of Toronto, Toronto, Canada

ABSTRACT The extracellular space of the glomerular capillary wall is occupied by a complex meshwork of fibrous molecules. Little is understood about how the size, shape, and charge recognition properties of glomerular ultrafiltration arise from this space-filling fiber matrix. We studied the problem of size recognition by visualizing the void volume accessible to hard spheres in computer-generated three-dimensional homogeneous random fiber matrices. The spatial organization of the void volume followed a complex "blob-and-throat" pattern in which circumscribed cavities of free space within the matrix ("blobs") were joined to adjacent cavities by narrower throats of void space. For sufficiently small solutes, chains of blobs and throats traversed the matrix, providing pathways for *trans*-matrix permeation. The matrices showed threshold or gating properties with respect to permeation: solutes whose radius exceeded a critical value, at which a throat on the last connected *trans*-matrix pathway pinched off, could not cross, whereas smaller solutes had nonzero permeability. The thresholds may give the glomerular fiber matrix porelike response properties and explain why pore models have been such a useful means of treating glomerular permselectivity.

INTRODUCTION

In the heteroporous model of glomerular size selectivity set out by Deen et al. (1), the best fit to neutral dextran clearance data in healthy and proteinuric patients comes from a model in which the glomerular capillary wall contains two classes of rigid, cylindrical pores. There are pores of small radius ($\approx$55 Å), through which most of the bulk flow takes place. These pores are numerous compared with the second class, which contains the "shunts." A shunt is a pore of very large (effectively infinite) radius. Shunts offer negligible resistance to bulk flow and to solute flux, including plasma proteins and other large macromolecules. Normally, shunts are sufficiently few in number that neither the bulk flow nor the solute flux through them is significant. Proteinuria is caused by an increase in the abundance of shunts, together (possibly) with a reduction in the negative charge density of the material forming the glomerular capillary wall. Excellent fits to clearance data from human patients with proteinuria and animal models of the nephrotic syndrome are obtained with this model, which has been widely applied to interpret functional lesions of glomerular ultrafiltration in terms of structural change (1–7).

Several decades of morphological study have, however, failed to demonstrate pores or channels penetrating the glomerular capillary wall, as required by these models. Instead (8, 9), they show two cell layers separated by a basement membrane (Fig. 1). Solutes crossing the glomerular capillary wall must pass through the matrix of fibrous molecules forming the basement membrane and filling the spaces between the cells. Little is currently known about how the structural properties of these fiber matrices can be used to explain the solute size, charge, and shape recognition properties of glomerular ultrafiltration, together with the obvious efficacy of the pore models.

In the native state, the fiber matrix of the glomerular capillary wall is assembled from a variety of macromolecules (8–22). No data are available that describe the exact three-dimensional organization of these macromolecules in vivo. However, recent modeling studies of transcapillary flux in the glomerulus (23–25) and other microvascular beds (26–29) have established that a simple structural model of matrix organization, due to Ogston et al. (30, 31) and placed on a firm basis in kinetic theory by Giddings and co-workers (32), provides a good initial fit to in vivo bulk flow and solute permeability behavior. In the Ogston model, the matrix consists of randomly oriented, rigid, homogeneously distributed fibers of uniform effective steric radius r_f. Fibers are packed into the matrix until the void volume is ϵ.

In this paper we present a computer-based study of the way the space accessible to solutes is organized inside a fiber matrix layer parameterized by r_f and ϵ. The solutes are treated as hard spheres of radius equal to their Stokes–Einstein hydrodynamic radius. The region accessible to solutes moving through the matrix is visualized using three-dimensional computer graphics. The manner in which the spatial organization of the void volume changes as solute size is varied suggests that the fiber matrix layer has a percolation threshold (33) that gates solute ultrafiltration. Solutes larger than a critical size equal to the percolation threshold cannot cross it; no ultrafiltration pathways through the matrix are available and the neighborhood is impermeable. Solutes of radius smaller than the percolation threshold value can cross the matrix. These permeating solutes sweep out irregular, pore-like channels of excluded volume as they pass among the fibers.

Our findings confirm and extend earlier work (34, 35), based largely in the chromatography literature (32,

J. W. Booth's present address is Biophysics Program, Harvard University, Cambridge, MA 02138.
Address correspondence to Charles J. Lumsden.

0006-3495/93/06/1727/08 $2.00

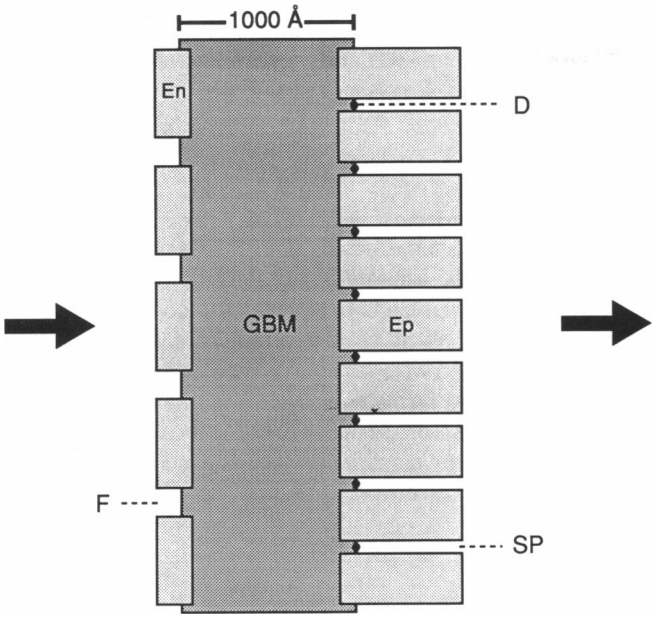

FIGURE 1 The glomerular capillary wall in cross-section. In this schematic, *En* denotes endothelial cell body, *F* an endothelial fenestra, *Ep* a foot process of a glomerular visceral epithelial cell, *SP* a slit pore (region between adjacent foot processes), *D* a glomerular slit pore diaphragm, and *GBM* the trilaminate glomerular basement membrane. Components roughly to scale. (*Large black arrows*) Direction of solute and volume flux.

36–38), establishing the existence of abrupt size cutoffs in fiber matrix permeability. These studies have applied the methods of statistical mechanics, and so provide a comprehensive view of how the average solute exclusion properties of a fiber matrix are determined by the statistics of its void volume distribution. The implications of this cutoff behavior for better understanding glomerular permeability and pore theory have recently been discussed by Schnitzer (25). In a pore model, solutes of radius exceeding the pore radius cannot enter the transmembrane channel and are excluded. Smaller solutes can enter the pore and their transport properties reflect their interactions with the pore wall. Pore models work well because the fiber matrix architecture of the glomerular capillary wall acts like a gate for sterically rigid solutes, excluding solutes above a specific size. The threshold value is distributed statistically along with the structural properties of the matrix (25, 35). Thus, threshold behavior in the glomerular capillary wall guarantees that pore theory is a reasonable first approximation to more realistic structural models based on fiber meshworks.

What has been missing from the development of these arguments to date is a method that translates the study of threshold or cutoff behavior down to the level of individual solutes and their interactions with the fiber matrix. Such methods obviously complement the statistical thermodynamic approach by providing detailed information on the spatial organization of the matrix void volume seen by individual permeants, and on the response of this spatial organization to changes in solute size, shape, or charge. We report here on our examination of size selectivity.

METHODS

Basic assumptions

For random fiber matrix models of the glomerulus and other capillary walls, $r_f \approx 5$–10 Å and $\epsilon \approx 93$–96% (23, 24, 26, 27, 29). We considered such matrices in relation to permeating solutes represented, as in the classic pore models (1, 3, 39), as uncharged hard spheres of radius r_m equal to the corresponding Stokes–Einstein radius.

The fibers in each computer-generated model were positioned by choosing points randomly within a volume V to act as origins through which the fiber axes passed. Random directions for each fiber axis were then selected (Fig. 2). We could obtain void volumes of 93–94% in these central regions by taking V as a cube of side 160 times the fiber radius r_f. The densest matrices we examined contained 480 fibers within this volume. To minimize the edge effects present in any matrix of a finite size, we used only the central 5% of V, a cube of width $60r_f$.

Modeling and visualization of the void space $\mathcal{S}$

The void space $\mathcal{S}$ lying outside the fiber interiors is the region of primary interest for questions about permeation and transport. Ogston (30) considered each point in $\mathcal{S}$ to lie at the center of a spherical cavity of radius r_s equal to the distance from that point to the surface of the nearest fiber. Call the void space formed by the union of all possible $r_s > r_m$ spherical cavities $\mathcal{S}_{r_m}$. Thus, $\mathcal{S}_{r_m}$ is the space within the matrix available to a spherical molecule of radius r_m. For a random isotropic network composed of very long fibers of negligible thickness, the number of fibers whose axes lie at a tangential distance between r_m and $r_m + dr_m$ of a point chosen randomly somewhere in the matrix is given by $4\pi r_m l$,

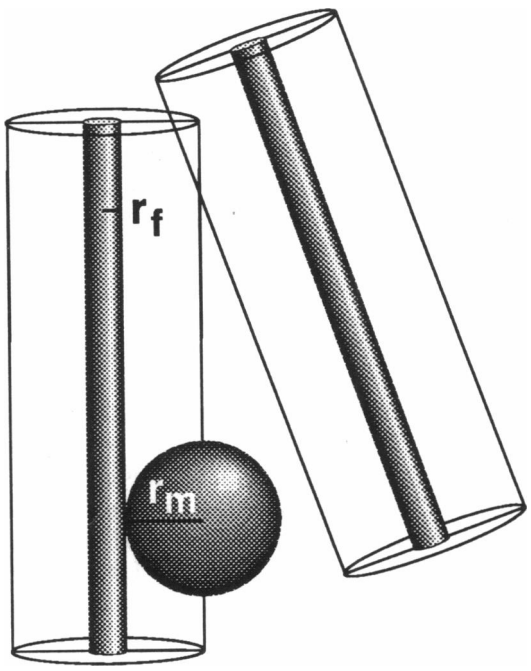

FIGURE 2 A spherical molecule of radius r_m is shown near two fibers of radius r_f. The outlined cylinders of radius $r_f + r_m$ are the surfaces of excluded volume, within which the center of a molecule cannot pass.

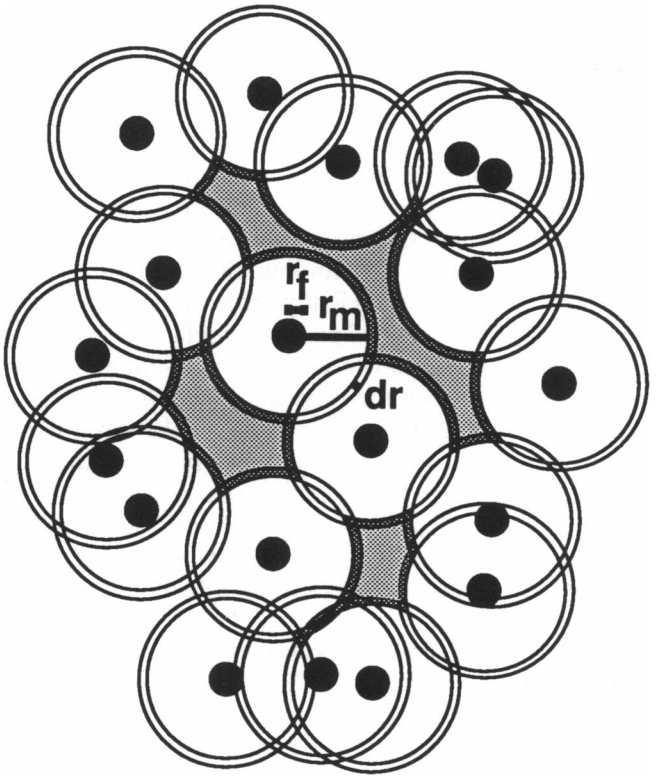

FIGURE 3 A two-dimensional analog of the void space $\mathcal{S}_{r_m}$ accessible to a molecule of radius r_m. The small, dark circles of radius r_f represent fibers. The total shaded area (dark and light together) is $\mathcal{S}_{r_m}$. The lightly shaded area is the space available to a molecule of radius $r_m + dr_m$. The large circles are analogous to the cylindrical surfaces of excluded volume in three dimensions (see Fig. 2). The locations at which these circles intersect, producing a convex point in the perimeter of the shaded areas, are analogous to ridges and points in the surface of a three-dimensional $\mathcal{S}_{r_m}$.

where l is the length of fiber per volume (30). The fraction of spherical spaces whose radii fall between r_m and $r_m + dr_m$ is then

$$\frac{dP}{dr_m} = 2\pi l r_m \exp(-\pi l r_m^2) \quad (1)$$

and so

$$P_{r>r_m} = \exp(-\pi l r_m^2) \quad (2)$$

is the probability that a spherical molecule of radius r_m can be placed at a point chosen at random in the matrix. In thermodynamic studies this probability is set equal to the partition coefficient of the solute, multiplied by that fraction of the total void available to water (27). In terms of the possible positions at which a molecule can be found, the case of a spherical molecule of radius r_m encountering fibers of radius r_f is equivalent to that of a spherical molecule of radius $r_m + r_f$ encountering fibers of zero radius (Fig. 2). In both cases, the closest possible approach of the center of a molecule to the axis of a fiber is $r_m + r_f$.

For each fiber matrix we simulated, a cubic lattice of points was constructed in the $(60r_f)^3$ box located at the matrix center. The perpendicular distance from each lattice point to the nearest fiber surface was calculated, giving the radius r_s of the spherical cavity centered on each point. From the Ogston construction the void space of the fiber matrix can be mapped into a set of nonintersecting surfaces, on each of which the value of r_s is constant (Fig. 3). The values of these radii provide a three-dimensional contour map of the void space. For each solute radius r_m we mapped $\mathcal{S}_{r_m}$ by identifying the subset of lattice points for which the distance to the nearest fiber is $\geq r_m$. Visualizing this subset of lattice points provided a readily inspected model of $\mathcal{S}_{r_m}$. A lattice spacing of one fiber radius proved adequate to visualize the three-dimensional form of these contour surfaces over the range of solute sizes applied in our study.

If the matrix regions sampled in our lattice approximation to $\mathcal{S}_{r_m}$ constitute a matrix interior of the type described by Ogston, the fraction F of all lattice points that lie in $\mathcal{S}_{r_m}$ is distributed as $\exp[-\pi l(r_m + r_f)^2]$. We therefore tested the null hypothesis that F satisfied this distribution. The computer resources available to us permitted F to be sampled at 26 values of r_m across a sample of 21 different matrices, and a χ^2 test for goodness of fit applied.

Connectivity and percolation thresholds in $\mathcal{S}_{r_m}$

As molecular radius $r_m \to 0$, $\mathcal{S}_{r_m}$ will in general be a connected region: any two points lying outside the fiber interiors can be connected by a path lying entirely in the void space and $\mathcal{S}_{r_m}$ runs contiguously through the fiber matrix. As r_m increases, so does the radius $r_m + r_f$ of the cylindrical volumes from which the center of the molecule is excluded. As r_m continues to increase, solute size may reach a threshold value r_c beyond which $\mathcal{S}_{r_m}$ breaks into a number of smaller unconnected regions, among which permeation is impossible (a percolation threshold; e.g., reference 33).

We looked for evidence of percolation thresholds with the following procedure. Each point in the cubic lattice of sampling points has $3^3 - 1 = 26$ immediately adjacent neighbors. Consider a lattice point lying inside the void region $\mathcal{S}_{r_m}$. If one of its 26 neighbors was also in $\mathcal{S}_{r_m}$, the two points were considered to lie in the same cluster of points. This cluster represents a contiguous subsection of $\mathcal{S}_{r_m}$. By applying this adjacent neighbor criterion recursively over the set of all lattice points, we could identify for each point in $\mathcal{S}_{r_m}$ the specific cluster to which it belonged; the number of clusters and their sizes could thus be surveyed.

The clustering procedure was applied to 46 different matrices, the maximum number accessible with the computer resources available to us. For each matrix the solute size was varied from $0r_f$ to $10r_f$ in $0.1r_f$ increments. On each block of fiber matrix the algorithm identified an upstream face and the opposing, downstream face. Our rationale for distinguishing two of the six structurally identical faces of the fiber matrix block was to refer the block to the environment of the glomerular capillary wall and the process of glomerular ultrafiltration, which carries solutes from the interior of the glomerular capillary across the filtration barrier and into Bowman's space. The convective flow of plasma water across the barrier produces a natural direction of solute motion, upon which is superimposed diffusive displacements within the liquid environment of the ultrafiltrate. We therefore associated one face of the simulated fiber matrix block with the (subendothelial) ultrafiltration surface facing the blood, and one with the (subepithelial) surface facing the urine, then focused on the contiguity of $\mathcal{S}_{r_m}$ with respect to these upstream and downstream faces: the smallest value of the solute molecule radius r_m for which a continuous path through the void space $\mathcal{S}_{r_m}$ no longer joined the upstream and downstream faces was adopted as the method's estimate of the percolation threshold r_c. The other four faces of the fiber matrix block were envisaged as abutting identical adjacent blocks of fiber matrix, and so on ad infinitum, thus emulating the layer-like organization of the glomerular basement membrane. No special status was assigned in this study to pathways in $\mathcal{S}_{r_m}$ connecting the upstream face to any of these side faces. In so doing we reasoned that the path length from upstream face to downstream face in the block was, for a given r_m, typically shorter than path lengths requiring the solute molecule to exit from the block into neighboring blocks before attaining the downstream face. Thus, dealing with the $\mathcal{S}_{r_m}$ paths joining the upstream and downstream faces would give a useful first estimate of the size recognition behavior of a laterally extended fiber matrix layer. It was also apparent (see Discussion) that solutes

whose size approximates that at which the glomerular basement membrane prohibits solute passage would have insufficient time to diffuse laterally out of the initial fiber matrix block during ultrafiltrative transit across the glomerular capillary wall.

RESULTS

The fraction F of lattice sampling points lying in $\mathcal{S}_{r_m}$ for a given solute radius r_m fitted the distribution predicted for matrices of the kind described by Ogston (30) for each of the 21 matrix interiors we examined. The characteristic behavior of F was sigmoid, with $F \rightarrow 1$ for small molecular radii and $F \rightarrow 0$ as molecular size increased. In every case, the null hypothesis that F came from the predicted distribution could not be rejected at the 0.005 level of significance (min $\chi^2 = 4.97 \times 10^{-6}$, max $\chi^2 = 6.50 \times 10^{-4}$, 26 degrees of freedom). Because we could not reject the null hypothesis, we treated the computer-generated fiber matrices as blocks of random fiber matrix of the Ogston type. The value of l, the length of fiber per unit volume, varied over the different matrix sections, with a mean value ± standard deviation of $0.0226 r_f^{-2} \pm 0.0022 r_f^{-2}$ and a corresponding void volume of 93.25 ± 0.59%.

Upon visualization the fiber matrices were dense meshes. $\mathcal{S}_{r_m}$ had a complex structure characterized by irregularity and significant surface evagination. The surface evaginations had the form of narrow "throats" of void volume, which often connected larger, circumscribed cavities or blobs of void volume to each other (Fig. 4).

The structure of $\mathcal{S}_{r_m}$ was a sensitive function of the solute molecular radius and the fiber radius. For molecules $< 4r_f$ the largest single cluster of lattice sample points in $\mathcal{S}_{r_m}$, which in general stretched from one side of the matrix to the other, accounted for >50% of all the sample points in $\mathcal{S}_{r_m}$. As molecular radius r_m increased, the throat regions of void volume in $\mathcal{S}_{r_m}$ narrowed progressively, until at a threshold value $r_m = r_c$ at least one throat on the last connected pathway crossing the matrix via $\mathcal{S}_{r_m}$ pinched off. At that point at least two separate void regions were formed from the single region originally forming $\mathcal{S}_{r_m}$ (Fig. 4). Breakdown of this largest cluster occurred at threshold values in the range $r_c = 4r_f$ to $6r_f$ for sections of matrix with void volumes in the range 96–97% (Fig. 5).

The distribution of thresholds was unimodal over the range of molecular sizes examined (Fig. 5). For effective fiber radii r_f in the range 5–10 Å, the distribution's mode, $5r_f$, corresponds to a solute size threshold value r_c in the range 25–50 Å. A distance of $60r_f$, the maximum we could examine with the computer resources at our disposal, runs one-third to one-half the way across the murine glomerular capillary wall. For longer permeation distances through matrices of the same void volume and fiber dimensions, the distribution of percolation thresholds would be shifted toward somewhat lower values and smaller solutes, because some regions of $\mathcal{S}_{r_m}$ that span a $60r_f$ matrix will not always span longer distances.

DISCUSSION

We verified that the partition coefficient for the computer generated matrices satisfied the predicted theoretical expression for spherical molecules in random fiber matrices. However, the finding that $\mathcal{S}_{r_m}$ breaks into smaller clusters for sufficiently large r_m raises questions concerning this predicted partition coefficient. Although the total volume into which a spherical solute of radius r_m will fit does obey the predicted $\exp(-kr_m^2)$ distribution, the volume that is accessible, in the sense that a molecule can move between any two points in that volume, can only be as large as the largest individual cluster. Taking this as a definition of accessibility, the thermodynamic partition coefficient (for review see reference 27) overestimates the truly accessible void volume for large, rigid solutes (35).

The matrix permeability was constrained by the overall connectivity of $\mathcal{S}_{r_m}$. In the random fiber matrix, this connectivity varied with solute size. As r_m increases, $\mathcal{S}_{r_m}$ gradually breaks up into unconnected volumes. At the critical solute radius $r_m = r_c$, the last connected pathway through $\mathcal{S}_{r_m}$ joining the upstream face to the downstream face of the fiber matrix block is ruptured. For solute molecules of size $r_m \geq r_c$ the barrier is impermeable. At intermediate values of r_m this is a decreasing number of pathways through the block, each with progressively smaller throat regions connecting the blobs. As r_m increases through these intermediate values, there are three readily identifiable effects on the permeation pathways. First, the constrictions along the void volume pathways tighten. Second, branching connections between parallel pathways decrease. Third, the mean length of the remaining pathways increases, as the shape of $\mathcal{S}_{r_m}$ becomes more tortuous before finally breaking up. This expected increase in mean path length itself decreases the permeability of the matrix. Because there is statistical fluctuation in matrix organization among the simulated blocks of fiber matrix, the percolation threshold in a larger system like the glomerular capillary wall is a statistical quantity whose distribution could be characterized by repeated sampling of the allowed matrix geometries (Fig. 5).

The glomerular basement membrane width in the rat and human nephron is 1000–3000 Å (15, 18) and the speed of convective flow across the wall is on the order of SNGFR/S, where SNGFR is the single nephron glomerular filtration rate and S is the surface area per glomerulus available for ultrafiltration. For the rat this gives $\approx 10^5$ Å/s with SNGFR $\approx$ 40 nl/min and S $\approx$ 0.0015 cm^2 (1, 2, 14). For the dog under mannitol diuresis the glomerular filtration rate (GFR) is $\approx$50 ml/min per 2×10^5 nephrons (40), so SNGFR/S is roughly 5–10 times that in the rat if S has the same order of magnitude. For

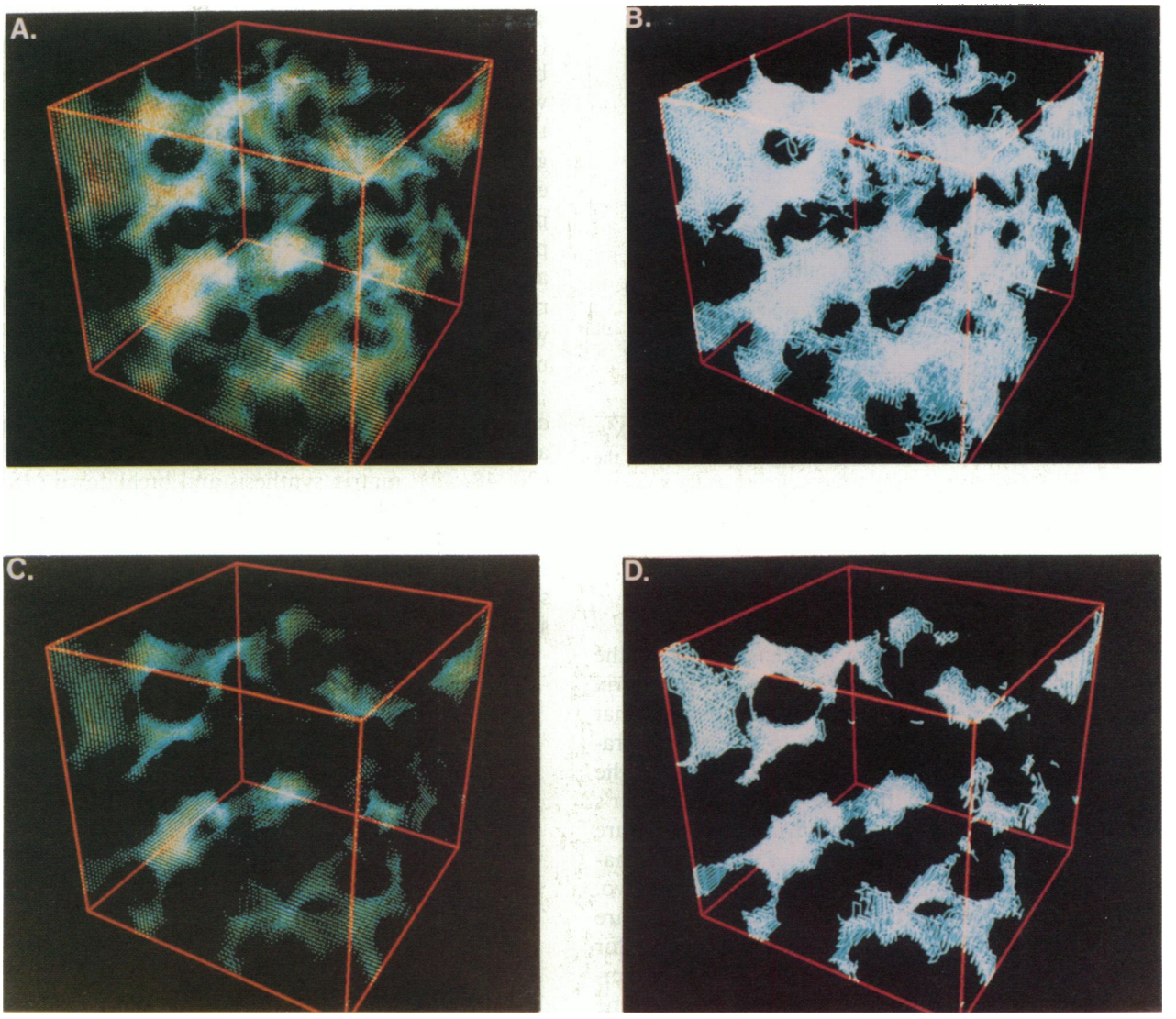

FIGURE 4 (*A*) The void space $\mathcal{S}_{r_m}$ visualized for a matrix with void volume 93.04%. The radius of the permeating molecule is four times the fiber radius. Pixels closer to the red end of the spectrum denote greater distance from the pixel location to steric contact with the nearest fiber. (*B*) The connectivity of $\mathcal{S}_{r_m}$ in *A* illustrated by drawing lines connecting points within a cluster. With $r_m = 4r_f$, $\mathcal{S}_{r_m}$ consists primarily of one large cluster. (*C*) The void space $\mathcal{S}_{r_m}$ for $r_m = 5.5r_f$. (*D*) The connectivity of $\mathcal{S}_{r_m}$ for $r_m = 5.5r_f$. $\mathcal{S}_{r_m}$ has broken into isolated clusters.

an ideal solution of Stokes–Einstein spheres at 37°C the free diffusion coefficient D_∞ has magnitude $0.0000328/r_m$ cm^2/s if r_m is measured in angstroms. The value of the solute diffusion coefficient in the fiber matrix, D_{FM}, is $< D_\infty$. Assuming that solute access to the void space decreases smoothly with increasing solute size in a fiber matrix of void volume ϵ and effective fiber radius r_f (i.e., ignoring percolation threshold effects), the ratio D_{FM}/D_∞ is $\exp[-(1-\epsilon)^{0.5}(1 + r_m/r_f)]$ (27). For a small solute ($r_m = r_f$) this factor is 0.6. The mean square Einsteinian diffusion distance the permeating solute can travel laterally in the plane of the fiber matrix layer during the time t it convects across the layer is $2tD_{FM}$. This corresponds to a laterally extended patch of the fiber matrix layer several hundred of our blocks on a side (Fig. 6).

Intriguingly, patch size decreases rapidly as solute size increases. For example, when $r_m = 9r_f$, D_{FM}/D_∞ is ~ 0.1. This is a significant restriction, but it is clearly an underestimate of the reduction in mobility because any solute bigger than $\sim 5r_f$ (roughly the size of albumin; e.g., see reference 41) exceeds the percolation threshold radius in these matrices. The likelihood of the $9r_f$ solute finding a path leading outside the block it first contacts is essentially zero. Thus for macromolecular solutes whose size approaches or exceeds the percolation threshold radius a patch consists of at most a small number of contiguous fiber matrix blocks of the size studied here.

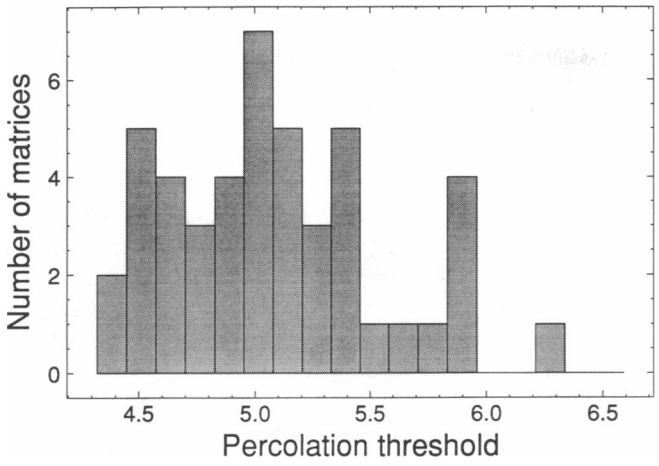

FIGURE 5 Distribution of percolation thresholds for a sample of $N = 46$ fiber matrices. The percolation threshold r_c was taken to be the maximum value of solute molecular radius r_m for which there exists a part of $\mathcal{S}_{r_m}$ spanning the matrix (see Fig. 4 and text for further discussion). The percolation threshold is expressed in multiples of the fiber radius r_f.

For effective fiber radii r_f in the range 5–10 Å, the mean size of the largest solute passed by our fiber matrix blocks, $5r_f$, is 25–50 Å. This range of values overlaps that (45–55 Å) assigned by pore models to the effective radius, r_p, of the small pores (e.g., 1, 3, 42–44). In the studies carried out since the time of Pappenheimer's classic work (42), the combination of micropuncture and clearance methods has provided detailed information on the ultrafiltration properties of glomeruli in vivo. Representative values for the (Munich Wistar) rat are $K_f = 0.07$ nl/s mmHg per glomerulus and $r_p \approx 50$ Å for neutral dextran solutes with $r_m > 28$ Å (43). In the simplest case, corresponding to isoporous membrane theory, the glomerular ultrafiltration coefficient K_f is $(S'/\ell)(r_p^2/8\eta)$ (43, 44), where η is the viscosity of water at 37C, S' is the total pore area per glomerulus, and ℓ is the effective thickness of the glomerular permeability barrier (effective pore length). For the representative values extracted from Chang et al. (43), this relationship gives $(S'/\ell) \approx$ 12–13 cm (ibid., 1975, Fig. 5). Taking $(S'/\ell) = 13$ cm, $\ell = 2{,}000$ Å and $r_p = 50$ Å leads to 3.3×10^9 pores per glomerulus. Distributing the 3.3×10^9 pores uniformly over the $S = 0.0015$ cm^2 of the peripheral glomerular capillary bed abutting basement membrane (14), one finds that each pore occupies a square unit cell of filtration surface of side length 200 Å. Our calculations indicate that fiber matrix regions of this size show distinct percolation threshold behavior.

Matrix regions with these dimensions also match the rectangular apertures ($\approx$40 Å $\times$ 140 Å; 10, 12–14, 21) observed in the slit pore diaphragm. If there are analogous openings in the in vivo slit pore diaphragm, the glomerular capillary wall may be functionally equivalent to serial assembly of gates (14, 45–47). The rectangular aperture of the slit pore diaphragm is the middle element in the assembly. On either side are fiber matrix regions (endothelial glycocalyx and glomerular basement membrane upstream; podocyte glycocalyx downstream) whose percolation thresholds and effective pore geometries regulate solute traffic to and from the slit pore region. Although much further work with improved models is clearly required, the hypothesis motivated by the present study is that the match among the gate regions in percolation thresholds ($\approx$55 Å) and in cross-sectional area ($\approx$100 Å $\times$ 100 Å) may explain why small pores running all the way through the glomerular capillary wall are such a useful starting point for modeling glomerular permselectivity.

The structural model used in our study is the simplest conceivable approximation to a basement membrane and leaves questions about nonrandom matrix structure (20, 48, 49), matrix synthesis and breakdown (18, 19, 49–51), conformational flexibility of matrix and solutes (39, 52–54), charge and shape recognition (3, 24), the explicit role of the slit diaphragms (47), and more extensive computational mapping of the models' parameter space open for future study. These remain to be devel-

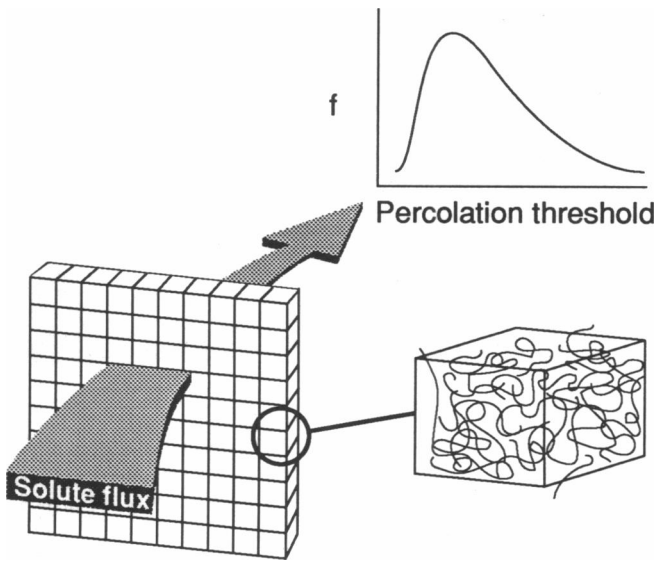

FIGURE 6 A glomerular capillary wall, functioning as a set of adjacent, contiguous patches, depicted for simplicity as square unit cells. A patch is the region of fiber matrix that a solute molecule can access by diffusion during the time it spends being ultrafiltered across the glomerular capillary wall. In the text we estimate that for macromolecular solutes the size of albumin a patch contains no more than several blocks of fiber matrix of the size studied in our simulations, whereas the patches seen by small solutes (e.g., the size of the fiber radius) measure $\approx 100 \times 100$ blocks. We suggest that each patch has a specific percolation threshold, r_c, and is impermeable to molecules of radius $r_m > r_c$. In the fiber matrix layer as a whole, percolation thresholds of magnitude r_c are present with frequency $f(r_c)$, where $\int_0^\infty f(r_c)dr_c = 1$. Thus pore models give a viable, though strictly phenomenological, approximation to glomerular ultrafiltration because a rigid pore with a fixed radius is the simplest ultrafilter structure with a percolation threshold for hard spheres.

oped. Although *trans*-matrix channels (shunts; references 1, 55, 56) large enough to readily pass solutes the size of albumin are observable in our visualizations and simulations, at this time we know little about their abundance or their structural properties. The continued study of fiber matrix models therefore promises to add important new insights into the structural basis of glomerular ultrafiltration.

We thank Jim Bassingthwaighte, James Given, J. Rodney Levick, Brian Myers, and the reviewers for their valuable comments on this work. Anthony Zielinski provided essential help with the graphics programming and visualization algorithms, as did Judy Fitzgerald with the artwork.

The project was supported by Medical Research Council of Canada (MRC) Grant MT-8635 to C. J. Lumsden. C. J. Lumsden holds an MRC Scientist career development award.

Received for publication 18 March 1991 and in final form 21 January 1993.

REFERENCES

1. Deen, W. M., C. R. Bridges, B. M. Brenner, and B. D. Myers. 1985. Heteroporous model of glomerular size selectivity: application to normal and nephrotic humans. *Am. J. Physiol.* 249:F374–F389.
2. Deen, W. M., B. Satvat, and J. M. Jamieson. 1980. Theoretical model for glomerular filtration of charged solutes. *Am. J. Physiol.* 238:F126–F139.
3. Deen, W. M., C. R. Bridges, and B. M. Brenner. 1983. Biophysical basis of glomerular permselectivity. *J. Membr. Biol.* 71:1–10.
4. Myers, B. D., C. Peterson, C. Molina, S. J. Tomlanovich, L. D. Newton, R. Nitkin, H. Sandler, and F. Murad. 1988. Role of cardiac atria in the human renal response to changing plasma volume. *Am. J. Physiol.* 254:F562–F573.
5. Golbetz, H., V. Black, O. Shemesh, and B. D. Myers. 1989. Mechanism of the antiproteinuric effect of indomethacin in nephrotic humans. *Am. J. Physiol.* 256:F44–F51.
6. Guasch, A., H. Hashimoto, R. K. Sibley, W. M. Deen, and B. D. Myers. 1991. Glomerular dysfunction in nephrotic humans with minimal changes or focal glomerulosclerosis. *Am. J. Physiol.* 260:F728–F737.
7. Myers, B. D., A. Chagnac, H. Golbetz, L. Newton, S. Strober, and R. K. Silbey. 1991. Extent of glomerular injury in active and resolving lupus nephritis: a theoretical analysis. *Am. J. Physiol.* 260:F717–F727.
8. Andrews, P. 1988. Morphological alterations of the glomerular (visceral) epithelium in response to pathological and experimental situations. *J. Electron Microsc. Tech.* 9:115–144.
9. Whiteside, C. I., K. Prutis, R. Cameron, and J. Thompson. 1989. Glomerular epithelial detachment, not reduced charge density, correlates with proteinuria in adriamycin and puromycin nephrosis. *Lab. Invest.* 61:650–660.
10. Rodewald, R., and M. J. Karnovsky. 1974. Porous substructure of the glomerular slit diaphragm in the rat and the mouse. *J. Cell Biol.* 63:423–433.
11. Farquhar, M. G. 1975. The primary glomerular filtration barrier—basement membrane or epithelial slits? *Kidney Int.* 8:197–211.
12. Ryan, G. B., R. Rodewald, and M. J. Karnovsky. 1975. An ultrastructural study of the glomerular slit diaphragm in aminonucleoside nephrosis. *Lab. Invest.* 33:461–468.
13. Scheenberger, E. E., R. H. Levey, R. T. McCluskey, and M. J. Karnovsky. 1975. The isoporous substructure of the human glomerular slit diaphragm. *Kidney Int.* 8:48–52.
14. Shea, S. M., and A. B. Morrison. 1975. A stereological study of the glomerular ultrafilter in the rat: morphometry of the slit diaphragm and basement membrane. *J. Cell Biol.* 67:436–443.
15. Kanwar, Y. S. 1984. Biophysiology of glomerular filtration and ultrafiltration. *Lab. Invest.* 51:7–21.
16. Ryan, G. B. 1986. The glomerular filtration barrier. *In* Advances in Renal Physiology. C. J. Lote, editor. Croom Helm, London. 1–33.
17. Timpl, R., and M. Dziadek. 1986. Structure, development, and molecular pathology of basement membranes. *Int. Rev. Exp. Pathol.* 29:1–112.
18. Abrahamson, D. R. 1987. Structure and development of the glomerular capillary wall and basement membrane. *Am. J. Physiol.* 253:F783–F794.
19. Fouser, L. S., and A. F. Michael. 1987. Antigens of the human glomerular basement membrane. *Springer Semin. Immunopathol.* 9:317–339.
20. Yurchenko, P. D., and J. C. Schittny. 1990. Molecular architecture of basement membranes. *FASEB (Fed. Am. Soc. Exp. Biol.) J.* 4:1577–1590.
21. Hora, K., S. Ohno, H. Oguchi, T. Furukawa, and S. Furuta. 1990. Three-dimensional study of glomerular slit diaphragm by the quick-freezing and deep-etching replica method. *Eur. J. Cell Biol.* 53:402–496.
22. Takami, H., A. Naramoto, H. Shigematsu, and S. Ohno. 1991. Ultrastructure of glomerular basement membrane by quick-freeze and deep-etch methods. *Kidney Int.* 39:659–664.
23. Fraser, W. D., and A. D. Baines. 1989. Application of a fiber-matrix model to transport in the renal tubules. *J. Gen. Physiol.* 94:863–879.
24. Lumsden, C. J., and M. Silverman. 1990. Multiple indicator dilution analysis of the kidney. *Methods Enzymol.* 191:34–72.
25. Schnitzer, J. E. 1992. Fiber matrix model analysis: matrix exclusion limits define effective pore radius describing capillary and glomerular permselectivity. *Microvasc. Res.* 43:342–346.
26. Curry, F. E., and C. C. Michel. 1980. A fiber matrix model of capillary permeability. *Microvasc. Res.* 20:96–99.
27. Curry, F. E. 1984. Mechanics and thermodynamics of transcapillary exchange. *In* Handbook of Physiology, Section 2: The Cardiovascular System. Vol. IV, Microcirculation, Pt. I. E. M. Renkin and S. R. Geiger, editors. American Physiological Society, Washington, DC. 309–374.
28. Curry, F. E. 1986. Determinants of capillary permeability: a review of mechanisms based on single capillary studies in the frog. *Circ. Res.* 59:367–380.
29. Levick, J. R. 1987. Flow through interstitium and other fibrous matrices. *Q. J. Exp. Pathol.* 72:409–438.
30. Ogston, A. G. 1958. The spaces in a uniform suspension of fibres. *Trans. Faraday Soc.* 54:1745–1757.
31. Ogston, A. G., B. N. Preston, and J. D. Wells. 1973. On the transport of chain molecules through solutions of chain-polymers. *Proc. R. Soc. (Lond.) B Biol. Sci.* 333:297–316.
32. Giddings, J. C., E. Kucera, C. P. Russell, and M. N. Myers. 1968. Statistical theory for equilibrium distribution of rigid molecules in inert porous networks: exclusion chromatography. *J. Phys. Chem.* 72:4397–4408.
33. Stauffer, D. 1985. Introduction to Percolation Theory. Taylor and Francis, London. 124 pp.

34. Serwer, P., and S. J. Hayes. 1986. Exclusion of spheres by agarose gels during agarose gel electrophoresis: dependence on the sphere's radius and the gel's concentration. *Anal. Biochem.* 158:72–78.

35. Schnitzer, J. E. 1988. Analysis of steric partition behavior of molecules in membranes using statistical physics: application to gel chromatography and electrophoresis. *Biophys. J.* 54:1065–1076.

36. Tiselius, A., J. Porath, and P. Albertsson. 1963. Separation and fractionation of macromolecules and particles. *Science (Wash. DC).* 141:13–20.

37. Laurent, T. C., and J. Killander. 1964. A theory of gel filtration and its experimental verification. *J. Chromatogr.* 14:317–330.

38. Rodbard, D., and A. Chrambach. 1970. Unified theory for gel electrophoresis and gel filtration. *Proc. Natl. Acad. Sci. USA.* 65:970–977.

39. Bohrer, M. P., W. M. Deen, C. R. Robertson, J. L. Troy, and B. M. Brenner. 1979. Influence of molecular configuration on the passage of macromolecules across the glomerular capillary wall. *J. Gen. Physiol.* 74:583–593.

40. Whiteside, C. I., and M. Silverman. 1983. Determination of glomerular permselectivity to neutral dextrans in the dog. *Am. J. Physiol.* 245:F485–F495.

41. Carter, D. C., X.-M. He, S. H. Munson, P. D. Twigg, K. M. Gernett, M. B. Broom, and T. Y. Miller. 1989. Three-dimensional structure of human serum albumin. *Science (Wash. DC).* 244:1195–1198.

42. Pappenheimer, J. R. 1953. Passage of molecules through capillary walls. *Physiol. Rev.* 33:387–423.

43. Chang, R. L. S., I. F. Ueki, J. L. Troy, W. M. Deen, C. R. Robertson, and B. M. Brenner. 1975. Permselectivity of the glomerular capillary wall to macromolecules. II. Experimental studies in rats using neutral dextran. *Biophys. J.* 15:887–905.

44. Bohrer, M. P., W. M. Deen, C. R. Robertson, and B. M. Brenner. 1977. Mechanism of angiotensin II-induced proteinuria in the rat. *Am. J. Physiol.* 233:F13–F21.

45. Graham, R. C., and M. J. Karnovsky. 1966. Glomerular permeability. Ultrastructural cytochemical studies using peroxidases as protein tracers. *J. Exp. Med.* 124:1123–1134.

46. Venkatachalam, M. A., M. J. Karnovsky, H. D. Fahimi, and R. S. Cotran. 1970. An ultrastructural study of glomerular permeability using catalase and peroxidase as tracer proteins. *J. Exp. Med.* 132:1153–1167.

47. Daniels, B. S., E. B. Hauser, W. M. Deen, and T. H. Hostetter. 1992. Glomerular basement membrane: in vitro studies of water and protein permeability. *Am. J. Physiol.* 262:F919–F926.

48. Adamson, R. H. 1992. An extension of the fiber matrix model of vascular permeability. *Microvasc. Res.* 43:352–356.

49. Walton, H. A., J. Byrne, and G. B. Robinson. 1992. Studies of the permeation properties of glomerular basement membrane: cross-linking renders glomerular basement membrane permeable to protein. *Biochim. Biophys. Acta.* 1138:173–183.

50. Wolgast, M., and G. Öjteg. 1988. Electrophysiology of renal capillary membranes: gel concept applied and Starling model challenged. *Am. J. Physiol.* 254:F364–F373.

51. Nilson, R. H., and S. K. Griffiths. 1990. Wormhole growth in soluble porous materials. *Phys. Rev. Lett.* 65:1583–1586.

52. Jansons, K. M., and C. G. Phillips. 1990. On the application of geometric probability theory to polymer networks and suspensions. *J. Colloid Interface Sci.* 137:75–91.

53. Klein, J. 1990. The interdiffusion of polymers. *Science (Wash. DC).* 250:640–646.

54. Zwanzig, R. 1992. Dynamical disorder: passage through a fluctuating bottleneck. *J. Chem. Phys.* 97:3587–3589.

55. Ryan, G. B., and M. J. Karnovsky. 1976. Distribution of endogenous albumin in the rat glomerulus: role of hemodynamic factors in glomerular barrier function. *Kidney Int.* 9:36–45.

56. Ryan, G. B., S. J. Hein, and M. J. Karnovsky. 1976. Glomerular permeability to proteins: effects of hemodynamic factors on the distribution of endogenous immunoglobulin G and exogenous catalase in the rat glomerulus. *Lab. Invest.* 34:415–427.